MAGNETIC RESONANCE IN CHEMISTRY
Magn. Reson. Chem. 2005; **43**: S256–S266
Published online in Wiley InterScience (www.interscience.wiley.com). DOI: 10.1002/mrc.1684

MRC

High-frequency ESR at ACERT†

Keith A. Earle, Boris Dzikovski, Wulf Hofbauer, Jozef K. Moscicki and Jack H. Freed*

Advanced Center for ESR Technology (ACERT), Baker Laboratory, Department of Chemistry and Chemical Biology, Cornell University, Ithaca, NY 14853, USA

Received 10 May 2005; Revised 23 June 2005; Accepted 27 June 2005

High-field ESR offers many advantages in exploring fundamental questions of structure and dynamics in chemical, biological and physical samples. We provide a review of recent work performed at ACERT demonstrating the utility and flexibility of our methods for extracting both qualitative and quantitative information from a variety of systems. In particular, we emphasize the utility of multi-frequency ESR techniques for unraveling the details of the complex dynamical modes of proteins in solution and in heterogeneous systems such as lipid bilayers. We also include indications of directions for future work where appropriate. Copyright © 2005 John Wiley & Sons, Ltd.

KEYWORDS: high-field ESR; quasioptics; millimeter waves; protein dynamics; lipid bilayers

INTRODUCTION

Since the early 1980s, more and more laboratories have applied high-field ESR to the study of complex systems.[1–5] Over the years, the field has benefited from numerous technological advances in the state of the art. Researchers in the 1980s and 1990s exploited advances in superconducting magnet technology to build reliable spectrometers that could examine $g = 2$ systems up to and above 300 GHz.[6–8] In addition, the high-field ESR spectroscopist now has ready access to a variety of powerful, low-noise, stable and reliable millimeter wave sources,[9,10] detectors and transmission lines[11] suitable for pulse and CW work, in both commercial turnkey systems[12] and specialized home-built spectrometers.[13–16] These advances have greatly increased the reliability and flexibility of contemporary spectrometer designs. Furthermore, advances in spin-labeling techniques, principally site-directed spin labeling (SDSL),[17] as well as spin-label design[18] allow the ESR spectroscopist a hitherto unmatched degree of flexibility to optimize experimental design for studies of dynamics and structure in complex systems.

GENERAL FEATURES OF HIGH-FIELD ESR SPECTRA

One of the most important features of ESR spectra is that they are sensitive to the detailed behavior of the relaxation-inducing dynamic modes of the system when the spectral extent, measured in frequency units, is comparable to, or larger than, the rotational diffusion rate.[19] This condition defines the onset of the slow-motion regime. When rotational correlation times are very short, i.e. in the motional narrowing regime, only limited information is available from a spectrum, as the spectrum only reports on averaged interactions that are, to a large degree, independent of the details of the averaging process. These considerations are clearly operative in Fig. 1, where we show a series of simulated spectra from low frequencies through high frequencies for a 'typical nitroxide' spin label.

A nitroxide spin label with a rotational correlation time of 1.7 ns produces at, e.g. 15 GHz a spectrum that is motionally averaged, i.e. a simple, three-line, hyperfine spectrum. At 250 GHz, one is near the T_2 minimum for this particular correlation time. This is where the anisotropic terms in the spin Hamiltonian are comparable to the rotational diffusion rate, and there is not much spectral detail present. At higher frequencies, one begins to resolve the canonical turning points of the **g**-tensor in the spectrum as one approaches the rigid limit. The spectra are characteristic of isotropic tumbling, the simple model used for these simulations.

It is important to note that at the very highest frequencies shown in Fig. 1 the hyperfine interaction is poorly resolved, and the spectrum is dominated by the **g**-tensor anisotropy. At conventional ESR frequencies, e.g. 9 GHz or lower, the spectrum is dominated by the hyperfine interaction. Given that the hyperfine tensor is axial, or nearly so, and the **g**-tensor is rhombic, for nitroxide spin labels, one can resolve asymmetric diffusion modes in high-field spectra as we have demonstrated previously.[21] The identification and analysis of asymmetric diffusion modes is most convenient when one can use spectra at different frequencies to provide constraints on various models, as we and others have shown in studies of simple fluids.[21–23]

It is convenient to characterize the behavior of ESR spectra in the following way. If one is interested in slow overall and collective modes of motion, they can be most easily studied by careful analysis of low-frequency ESR spectra.[24,25] The magnitude of such modes can also be estimated by hydrodynamic theory and compared to the

†**Presented as part of a special issue on High-field EPR in Biology, Chemistry and Physics.**

*Correspondence to: Jack H. Freed, Advanced Center for ESR Technology (ACERT), Baker Laboratory, Department of Chemistry and Chemical Biology, Cornell University, Ithaca, NY 14853, USA.
E-mail: jhf@ccmr.cornell.edu

Copyright © 2005 John Wiley & Sons, Ltd.

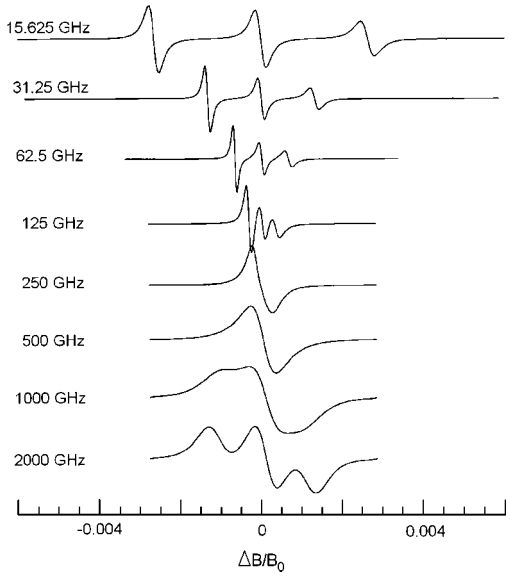

Figure 1. Simulated nitroxide spectra ($g_x = 2.009$, $g_y = 2.006$, $g_z = 2.002$; $A_x = 5.0$ G, $A_y = 4.0$ G, $A_z = 34$ G) corresponding to an isotropic rotational correlation time of 1.7 ns.[20] The spectra cover a broad range of frequencies as a function of spectral extent referenced to the central magnetic field. At the lowest frequencies, the spectra are in the motional narrowing regime. As the frequency increases, the spectra are more characteristic of the slow-motional regime. This is an example of what we call the snapshot effect, wherein processes that appear to be rapid on the ESR timescale at low frequencies appear slow on the ESR timescale at high frequencies. Above 35 GHz, the **g**-tensor anisotropy begins to dominate the spectra. At the very highest frequencies, the hyperfine interaction is not resolved, whereas at low frequencies, the spectrum is dominated by the hyperfine interaction.

results of spectral analysis.[26] If one is interested in rapid internal dynamic modes, then high-field ESR spectroscopy is very useful for the purpose; the slow modes, in favorable cases, will be frozen out on the high-field ESR timescale, leaving only the rapid internal modes corresponding to, e.g. backbone fluctuations in spin-labeled proteins to contribute significantly to the spectrum.[24,25,27] This is a manifestation of the so-called 'snapshot' effect.[19]

Rigorous spectral simulation and fitting techniques developed at ACERT now allow us to simultaneously analyze spectra taken at the same temperature but at different frequencies in a global spectral fitting approach in order to derive consistent sets of parameters for slow and rapid motional modes.[24,25] One can think of this as a logical extension of our work where we combined data sets at different frequencies to determine rigorously the asymmetry of the diffusion tensor in simple fluids.[21] Given that the dynamic modes of macromolecules are more complicated than those of small, rigid spin labels in simple fluids, one expects and observes that a more sophisticated model is necessary in order to determine reliable parameters.[24]

Recent theoretical work at ACERT has focused on developing and improving such sophisticated models. The dynamic cage or slowly relaxing local structure (SRLS) models allow for considerable freedom in the choice of model parameters that enter into a spectral fit.[28] Examples of a multi-frequency fit are shown in Fig. 2, where spectra at 9 and 250 GHz from a spin-labeled T4-lysozyme mutant were analyzed at the same temperature. The mutants studied had spin labels incorporated at the 72 and 131 positions. The complete analysis, incorporating fit results and their interpretation at a variety of temperatures has been published elsewhere.[29]

We are currently in the process of 'filling in' the frequency range studied for this system, taking advantage of the 95 and 170/240 GHz spectrometers recently constructed at ACERT. As an example of the kind of detail that we can now resolve, we show a series of spectra taken at a variety of temperatures and different frequencies (9, 95, 170 and 250 GHz) of T4-lysozyme labeled at the 131 site in Fig. 3. The model constraints provided by simultaneously fitting these spectra at each temperature taken at different ESR frequencies are expected to allow us to attain a very clear picture of the dynamic modes manifested in this system. We are currently performing the challenging task of simultaneous, nonlinear least-squares fitting of all these spectra.

FORMATION AND DISSOCIATION OF HEAD-TO-HEAD DIMERS OF GAS1 IN DPPC MEMBRANES

We have, so far, emphasized the information that high-field ESR can provide on dynamic modes in a given system, e.g. a protein. We would also like to emphasize that high-field ESR, because of its excellent orientational resolution, can provide insights into structural reorganization of complex systems such as peptides or proteins in membranes. Figure 4 shows spectra of spin-labeled gramicidin-A (GASl)

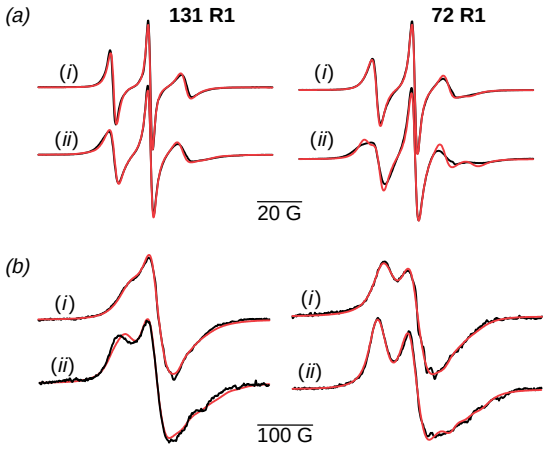

Figure 2. Simultaneous fits to ESR spectra from spin-labeled T4-lysozyme taken at (a) 9 and (b) 250 GHz.[24] The spectral fits (red) and the experimental spectra (black) are shown superimposed. The spectra in the left column are from the mutant labeled at the 131 site. Those in the right column are from mutants labeled at the 72 site: (i) 37.5 °C, overall rotational tumbling rate $R^c = 2.8 \times 10^7$ s^{-1} (ii) 10 °C, overall rotational tumbling rate $R^c = 1.5 \times 10^7$ s^{-1}. The 72-labeled spectra attest to higher internal ordering (and slower internal dynamical modes) compared to the 131-labeled spectra. The mutants were provided by our collaborator Wayne Hubbell of the Jules Stein Eye Institute at UCLA.

Copyright © 2005 John Wiley & Sons, Ltd.

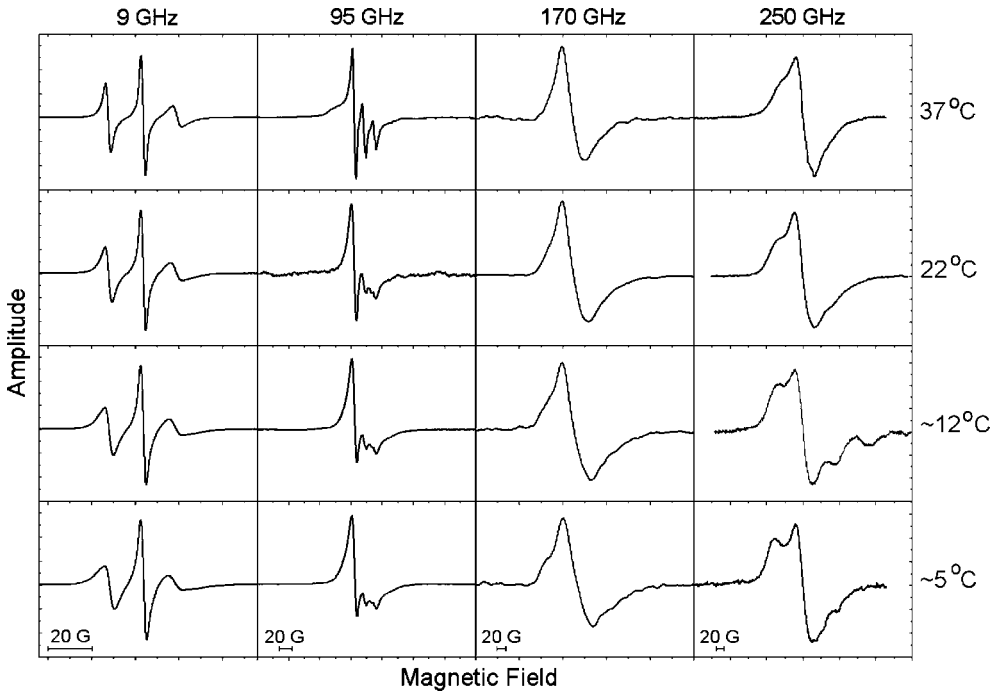

Figure 3. A multi-frequency ESR study of spin-labeled T4-lysozyme showing the significant spectral changes as the temperature is lowered (top to bottom) and the frequency is increased (left to right). These spectra were obtained from T4-lysozyme mutants labeled at the 131 position provided by Wayne Hubbell. Simultaneous analysis of the spectra at different frequencies is expected to resolve the spectral contributions from dynamic modes on different timescales. Note that as one increases the ESR frequency the spectra change in character from motionally narrowed to slow motional.

in macroscopically aligned membranes of DPPC. The peptide GA forms a transmembrane ion channel by dimerizing to form a head-to-head dimer.[29] Above the L_β–P_β lipid-phase transition, the ESR spectra indicate that GASl loses its *z*-ordering, which we interpret as arising from tilting of the nitroxides as the dimer channels are formed. When the temperature is lowered below the L_β–P_β transition, the *z*-ordering grows back with time as the dimers dissociate. We originally developed this model on the basis of detailed analysis of 9 GHz spectra.[29] However, the 170 GHz spectra in Fig. 4 demonstrate the effect in a more direct and transparent way, and they provide confirming evidence that this is indeed the result of membrane structural changes, given the vastly different timescales of the two ESR frequencies. The 170 GHz spectra also provide striking evidence of the effects of orderings of different symmetries on the spectral lineshape.

ORIENTATION-DEPENDENT EFFECTS IN LIPID BILAYERS STUDIED BY MICROTOME TECHNIQUES

One can also readily resolve orientation-dependent ordering effects in oriented lipid bilayers using a novel method developed at ACERT that allows one to collect spectra at several bilayer orientations with respect to the external magnetic field. Given the millimeter wave *E* and *B* field distributions imposed by our resonator geometry,[3,30] we have significant constraints on the sample geometry and position when studying aqueous samples. In order to keep the sample in regions of low *E* field (which minimizes dielectric losses) and high *B* field (which maximizes the ESR signal), we use sample holders that have so-called 'pancake' geometry.[31] The sample holder must then be aligned so that its symmetry axis is parallel to the optical axis of the resonator. All of these constraints preclude a traditional goniometer approach to studying the orientation-dependent spectra of aligned bilayers. We partially addressed this problem by constructing a shunt resonator that allowed us to obtain spectra from samples oriented perpendicular to the main field.[32] With this technique, however, intermediate orientations are not readily accessible. We have now developed a technique with which we can prepare individual samples that are oriented at a range of fixed angles with respect to the applied magnetic field, yet can be positioned and aligned for minimum dielectric loss in the resonator.

The basis of the new technique is to prepare a standard oriented lipid bilayer, using conventional isopotential spin-dry ultracentrifugation (ISDU) methods,[33] then freezing the sample and taking thin slices at a specified angle from the sample normal. The slices are taken using a scalpel under the control of a fine mechanical mechanism. We call this the 'microtome' technique. The procedure is outlined in Fig. 5. Representative spectra at 9 and 170 GHz are shown in Fig. 6 for GASl in oriented DPPC bilayers. We have also performed similar studies on 16PC and cholestane (CSL) in oriented DPPC bilayers. The angular dependence of the spectra allows us to characterize the details of the ordering in the system as we have shown in previous work.[34] We are preparing a report on this microtome technique for publication.[35]

Copyright © 2005 John Wiley & Sons, Ltd.

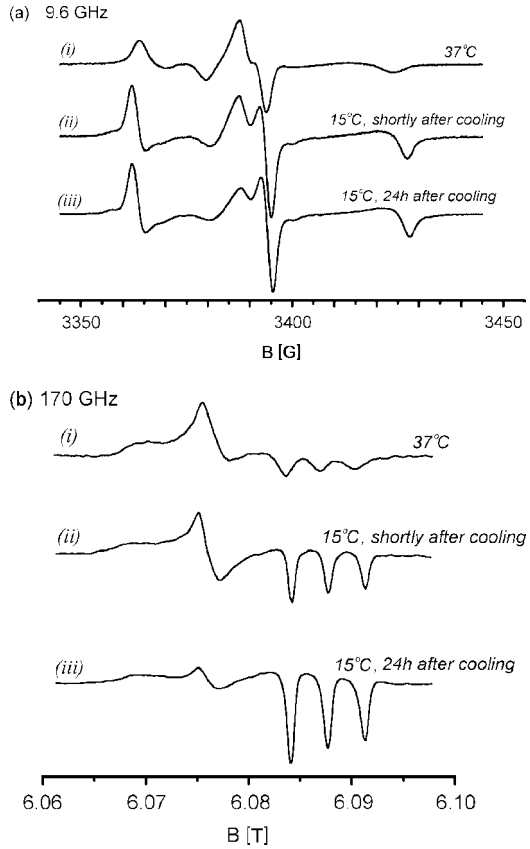

Figure 4. Spectra from spin-labeled gramicidin-A (GASI) in macroscopically oriented lipid (DPPC) bilayers at (a) 9.6 and (b) 170 GHz. The normal to the bilayers is parallel to the magnetic field. These spectra demonstrate the sensitivity of high-field ESR to ordering and orientation effects. At low temperatures, the GASI spectra attest to strong *z*-ordering (*cf* iii). When the temperature is raised above the L_β–P_β transition, (i) the spectral weight shifts to the *x* and *y* regions of the 170 GHz spectrum, which we interpret as a tilting of the nitroxide spin label due to the formation of head-to-head dimer channels in the P_β phase. Upon cooling the system below the L_β–P_β transition, we initially observe (ii) a 'hysteresis state' with ordering intermediate between the P_β and the L_β phase spectra. After a sufficiently long time (>24 h) the *z*-ordered spectrum (iii) reappears. The effects of these processes are not readily interpretable from the 9 GHz spectra, which required detailed analysis.[29]

DEVELOPMENTS IN SITE-DIRECTED SPIN LABELING (SDSL)

SDSL is being exploited by many as a technique for studying proteins and peptides that are otherwise ESR silent or have ESR spectra that are not well resolved.[36] The most popular spin label for SDSL work has been methanethio sulfonate spin label (MTSSL) which can be attached to a cysteine residue, natural or engineered, via a disulfide bond.[37] Motion of the spin label around the tether can complicate the interpretation of the resulting spectra, as the motion around the tether is only indirectly coupled to protein backbone motions or overall tumbling modes. A modified version of MTSSL with a methyl group at the 4 position of the nitroxide-bearing doxyl ring significantly hinders the tether motion so that ESR spectra resulting from this spin-label report more directly on protein dynamic modes.[37] Spectra at 95 and 170 GHz from T4-lysozyme labeled with both kinds of spin label are shown in Fig. 7. The spectra resulting from the methylated spin label clearly attest to slower motions than the unmethylated spin-label spectra. We infer, therefore, that the tether motions have been reduced in the Me-spin label spectra.

In addition to conventional SDSL techniques, there are a variety of 'unnatural' amino acids incorporating a nitroxide spin label, e.g. 2,2,6,6-tetramethyl-piperidine-N-oxyl-4-amino-4-carboxylic acid (TOAC), that are available for use by ESR spectroscopists.[38,39] Currently, synthesis of proteins with TOAC is a nontrivial matter for all but the smallest proteins. Nevertheless, the technique does show considerable promise. Furthermore, given that TOAC is incorporated directly into the structure of the protein as opposed to reporting on the protein dynamics through the coupling of the spin label via its tether, it is likely that TOAC-derived spectra, where obtainable, may lead to results that are less prone to ambiguities of interpretation. One *caveat* that should be noted, however, is that TOAC can interfere with native protein structure.

INSTRUMENTATION FOR PERFORMING CW HIGH-FIELD ESR

All of our spectrometers at high fields ($\geq$3 *T*) are based on quasioptical design techniques. Quasioptics is a design philosophy that is appropriate when diffraction effects must be accounted for but do not dominate the propagation properties of an optical transmission line. It corresponds to the first physical optics correction to a simpler geometrical optics description. Over a broad range of beam parameters, the physical optics approximation leads to a set of design equations that are almost as easy to use as geometrical optics.[38,40] Instead of a point focus, one has a diffraction-limited beam waist, corresponding to the minimum achievable spot size. Lenses and conic-section mirrors may be designed and used to keep the optical beam collimated and controlled.[40]

We show a conceptual layout of a typical quasioptical bridge in Fig. 8.[13] One of the interesting features of quasioptical systems is that the optics conserve the polarization state of the incident beam. We exploit this feature to encode the ESR response of the sample for ease of detection.[41] This method is similar in spirit to induction-mode detection,[42] first developed in an NMR context.[43] Using polarization-coding techniques, we excite the ESR resonance using, say, vertically polarized millimeter wave radiation. The ESR resonance absorption generates co- and cross-polarized components in response to the excitation.[15,42] The cross-polarized response may be separated from the incident beam by a high-efficiency polarizer and subsequently detected.[15,41]

With the experience we have gained over the years, we have settled on a 'house style' for our home-built CW spectrometers. We advocate the use of cryogenically cooled bolometric detection using a hot-electron InSb chip.[11] This allows the spectroscopist to use a variety of millimeter wave sources of different frequencies without requiring dedicated detectors at each frequency. This is a consequence of the

Copyright © 2005 John Wiley & Sons, Ltd.

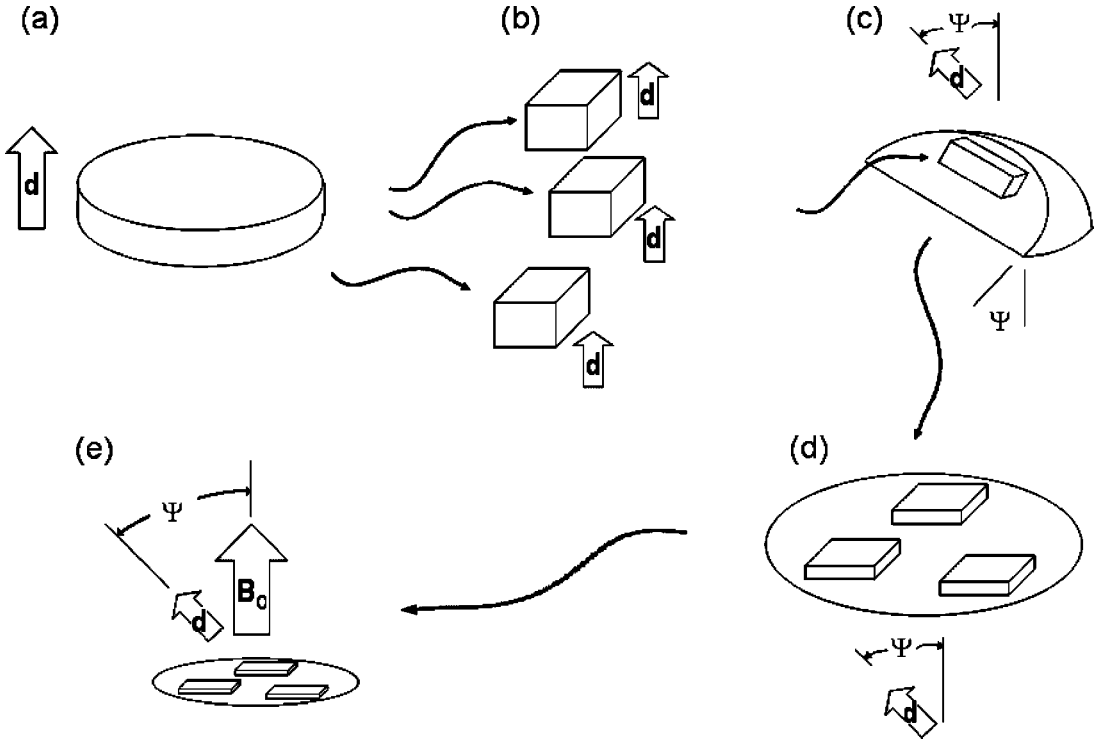

Figure 5. Schematic diagram of the microtome process. The first step in the process (a) involves preparing a multilamellar-oriented lipid bilayer membrane with appropriate spin-labeled membrane components using isopotential spin-dry ultracentrifugation (ISDU)[33] or some other technique such as pressure annealing. The ordering is characterized by the director **d**. One then removes sections of the sample (b) of a convenient size, e.g. 3 mm × 6 mm × 1 mm for mounting on a small block of ice (c) with a face at a predetermined inclination from the normal (ψ) which defines the tilt angle of the director **d** after the microtome slice has been prepared. After cutting, the microtome slices with tilt ψ are mounted on a millimeter wave transparent sample stage (d). Once a hermetically sealed sample is prepared, it may be mounted in the resonator (e) and spectra obtained for this value of tilt angle, ψ.

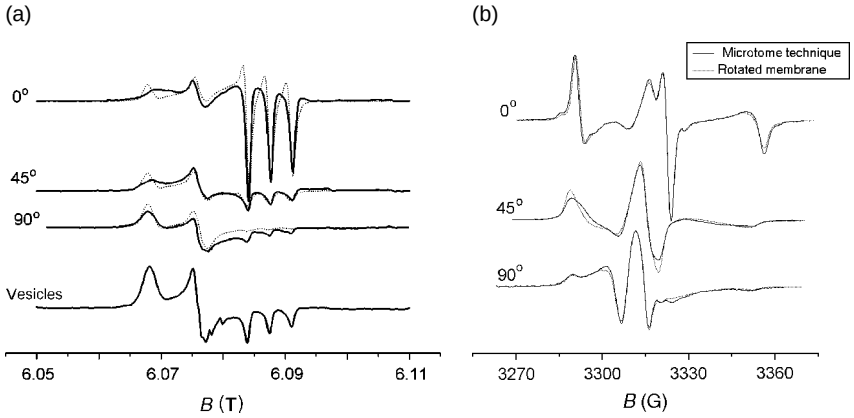

Figure 6. (a) 170 GHz ESR spectra of spin-labeled gramicidin-A (GASl) in macroscopically oriented (DPPC) bilayers (solid lines).[35] The dotted lines indicate spectral simulations. The bilayer director orientation with respect to the applied magnetic field is $\psi = 0^\circ$, 45°, and 90°. Both tilted samples were prepared by the microtome technique (*cf* Fig. 5). For comparison, a spectrum taken from spin-labeled gramicidin-A (GASl) in DPPC vesicles is shown at the bottom. (b) Validation of the microtome technique at X-band (9 GHz). Spectra (heavy lines) obtained from microtome samples with bilayer director orientation with respect to the applied magnetic field of 0°, 45°, and 90° are compared with spectra obtained from a perfectly aligned flat sample (light lines) placed in equivalent orientations.

broad frequency band over which the hot-electron bolometer has good responsivity, and, thus, good signal to noise.

At frequencies where solid-state sources are available (up to about 300 GHz), we recommend the use of multiplied sources derived from the output of a low phase-noise X-band solid-state source. With the efficient waveguide-based multipliers now available, it is possible to achieve approximately 40 mW of power at 170 GHz and 23 mW of power at 240 GHz,[9] as we have verified in our latest 170/240 GHz induction-mode ESR spectrometer.[14]

Copyright © 2005 John Wiley & Sons, Ltd.

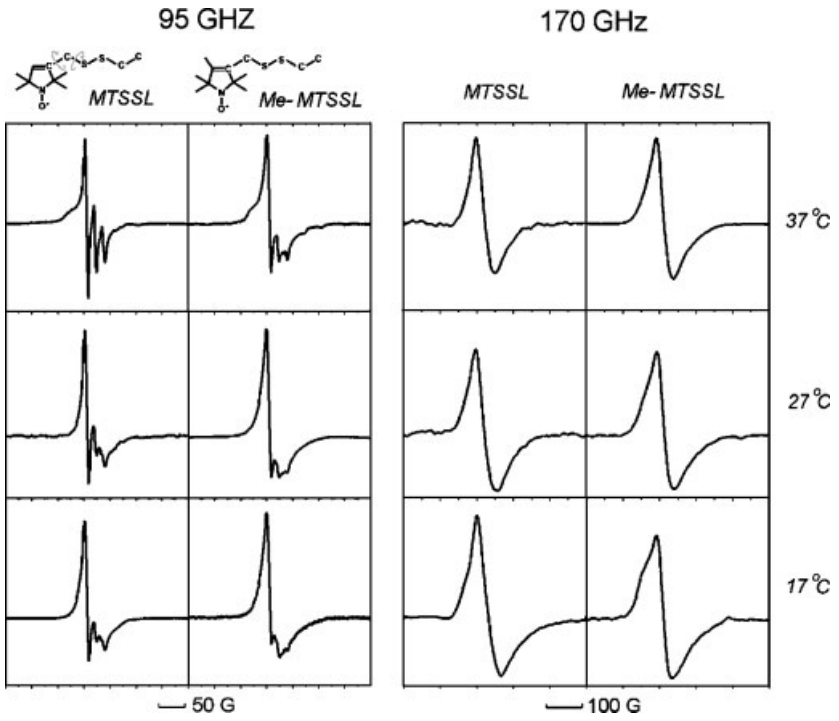

Figure 7. Comparison of spectra taken at 95 and 170 GHz, shown in separate panels, from MTSSL (a) and Me-MTSSL (b) labeled T4-lysozyme at the 131 site. Stick models are shown for both spin labels. For this particular set of conditions, the spectra are in the intermediate slow-motion regime, and there is modest sensitivity to the additional ordering provided by the methylation process.

We advocate the use of off-axis, conic-section reflecting optics, where possible, to minimize losses and the generation of astigmatic amplitude and phase errors in the quasioptical beam. When such mirrors are combined appropriately, the beam waist at the input and output ports of the mirror pair is independent of frequency, greatly simplifying bridge design.[38] Where reflecting optics cannot be used, because of space constraints, e.g. in the warm bore of a superconducting magnet, we recommend the use of a corrugated waveguide, which propagates a hybrid waveguide mode that preserves the polarization state of the incident quasioptical beam and couples efficiently to a free-space Gaussian beam mode.[40,41]

We have concentrated on the use of Fabry-Pérot resonators (FPRs) in our high-field ESR work as they have proven to be flexible in their application to particular design problems as well as straightforward to couple.[13,44] On the basis of these design criteria, we have built CW spectrometers that have achieved sensitivities of 10^8 spins/G for motionally narrowed spectra in a 0.3 Hz detection bandwidth.[45] For some applications, fundamental mode cavity resonators can offer advantages over the FPR approach, especially when the available power is limited but a substantial B_1 is required.[44,46] We have found that the open resonator approach is a useful one in studies of single crystals containing transition metal ions.[14,47–50]

PULSE ESR AT HIGH FIELDS

Up to this point, we have considered CW experiments. The possibility of manipulating coherences generated by pulse ESR at high fields provides an opportunity to study fundamental dynamical processes and probe static interactions that are difficult to observe and interpret with standard CW techniques.[19,51,52] In order to maximize the benefits of performing high-field pulse ESR, however, it is often necessary to generate intense B_1 fields of short duration. This is due to the fact that high-field ESR experiments, particularly in liquids, are characterized by T_2's on the order of nanoseconds and spectral extents of several hundred megahertz or more in the slow-motional regime where model sensitivity is expected to be the highest. Long, selective pulses will only partially excite the spectrum and diminish the multiplex advantage of pulse experiments using nonselective pulses.[53] Furthermore, when the pulse widths are significantly longer than the T_2's, the pulses will be rendered ineffective. Figure 9 shows a plot of predicted T_2 as a function of isotropic rotational tumbling rate at several frequencies for a 'typical' isotropically tumbling nitroxide. As the ESR frequency increases, the T_2 minimum shifts to faster tumbling rates and smaller absolute values. At 9 GHz it is 15 ns, whereas at 95 and 240 GHz, it is 4 and 1 ns respectively.

Owing to advances in millimeter wave source technology, we have successfully constructed a pulse/CW high-field ESR spectrometer at 95 GHz.[13] We were able to achieve a signal-to-noise ratio for pulse experiments of 10^{10} spins/$s^{1/2}$. The transmitter and receiver are combined into a common unit. It uses heterodyne techniques to optimize the detection sensitivity.[56] The maximum available CW power is 90 mW. It can be attenuated to lower levels, when desired, by means of a current-controlled p-i-n attenuator. For high-power pulse experiments, we drive a 1 kW Extended Interaction Klystron

Copyright © 2005 John Wiley & Sons, Ltd.

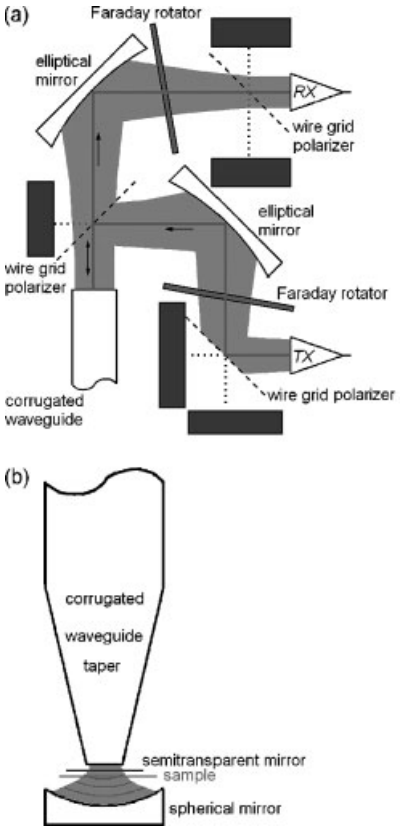

Figure 8. Schematic diagram of a typical quasioptical bridge: (a) transmit/receive duplexer based on polarization coding techniques.[13] A quasioptical beam is launched from the TX, or transmitter, port at the bottom right of the figure. The polarization purity of the beam is defined by the wire grid polarizer. The Faraday rotator, in conjunction with the wire grid polarizer, acts as an isolator to decouple reflected waves on the transmit arm from the TX port. The beam is refocused by the off-axis elliptical mirror. The wire grid polarizer at the input port of the corrugated waveguide reflects the beam from the TX port in the probe head. The ESR phenomenon generates reflected beams that are co- and cross-polarized. The cross-polarized beam is transmitted through the wire grid polarizer to the RX, or receiver, port. The off-axis elliptical mirror focuses the beam onto the RX port. The Faraday rotator and wire grid polarizer isolate the RX port from reflections on the receiver arm. This particular bridge is optimized for use at a frequency of 95 GHz. A broadband bridge would have elliptical mirrors configured in pairs to have frequency-independent beam waists at the input and output ports. We use this 'Gaussian telescope' technique in our 170/240 GHz bridge; (b) detail of ESR probe head showing the configuration of the Fabry-Pérot resonator (FPR) and flat sample geometry used in this work. The semitransparent mirror has continuously adjustable coupling in order to achieve critical coupling to a wide variety of samples. This utilizes our innovative design of a continuously variable coupling technique using overlapping meshes.

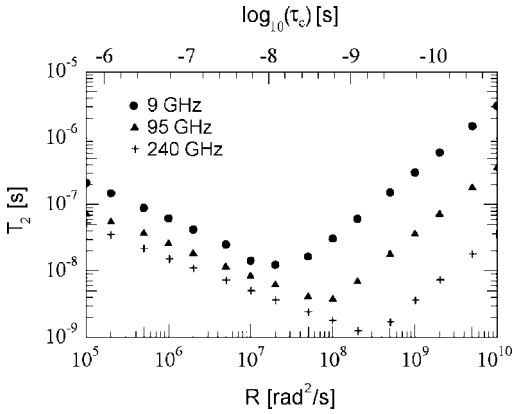

Figure 9. Plot of T_2 *versus* rotational tumbling rate as a function of ESR frequency for an isotropically tumbling nitroxide as calculated from the stochastic-Liouville equation.[54,55] Above the T_2 minimum, the homogeneous T_2 scales inversely with the rotational correlation time. The T_2 minimum shifts toward faster tumbling rates as the ESR frequency increases. At 95 GHz, it is approximately 4 ns. At 250 GHz, it is approximately 1 ns. This puts severe constraints on the allowable pulse length and deadtime of pulsed ESR spectrometers at high fields. However, at low temperatures, where the T_2 (and T_1) are very long, useful pulse experiments may be performed even with low-power devices which deliver much longer $\pi/2$ pulses.

Amplifier (EIKA) from CPI, Canada[10] with the output of our ELVA-1[56] transmitter. The use of the EIKA allows us to preserve the phase information encoded in the low-power drive pulses, which is necessary for the postdetection manipulation of coherences that we employ to extract the desired coherence pathways.

The spectrometer achieves 3–5 ns $\pi/2$ pulses corresponding to a B_1 of 1.7 mT (17 Gauss) for 5 ns pulses using an FPR.[13] A simple calculation shows that the available B_1 at the ESR sample scales as the square root of the available power for fixed resonator quality factor, Q_L. It is important to realize, however, that Q_L must be sufficiently small in order to faithfully transmit a short pulse, owing to bandwidth constraints. The available B_1 scales as the cube root of the available power when this is taken into account.[52]

The dead time is of the order of 30 ns under favorable conditions and can be reduced further for samples with very strong signals by attenuating the input to the receiver. Given the short T_2's at 95 GHz (*cf* Fig. 9), it is important to reduce the dead time as far as possible in order to register spectra in this motional regime, otherwise rapid relaxation effects will cause the signal intensity to decay to unobservable levels.

Near the T_2 minimum, it will be important to achieve even shorter $\pi/2$ pulses in order to avoid significant spectral relaxation during the course of the millimeter wave pulse. Work is underway in our laboratory on this technical issue. We advocate the use of a dielectric-loaded FPR to increase the available B_1 and reduce the time required for a $\pi/2$ pulse. Modeling results suggest that the available B_1 scales linearly with the dielectric constant (or index of refraction squared) of the dielectric loading the FPR.[57]

The spectrometer also has the ability to perform quadrature phase shift keying during a pulse sequence. In this way, we can select desired coherences and ameliorate spectral artifacts from undesired coherences. We have successfully performed 2D-ELDOR experiments on samples with limited

Copyright © 2005 John Wiley & Sons, Ltd.

spectral extent, e.g. nitroxides in the motional narrowing regime, (*cf* Fig. 10) as well as highly ordered spectra from spin labels in macroscopically aligned samples (*cf* Fig. 11).

Note in particular the presence of substantial cross-peaks that change with mixing time in Fig. 11. We tentatively ascribe these cross-peaks to the effects of the ^{14}N nuclear modulation, i.e. they are coherence cross-peaks.[58] At 95 GHz, the ^{14}N Zeeman interaction becomes close-in value to that of the ^{14}N hyperfine tensor (i.e. $\omega_N \approx A_{yy}$), which enhances the formation of such coherence cross-peaks. Since the relevant component of the CSL ^{14}N hyperfine tensor is substantial in this orientation ($A_{yy} \approx 5$ G), one requires the short and intense pulses that were used to excite all the allowed and forbidden hyperfine transitions at the *y*-orientation to produce such coherence cross-peaks.[58] It is also consistent with the CSL in DPPC at 7C being nearly rigidly aligned, so it is almost single-crystal like, also a requirement for developing such strong cross-peaks. The variation in intensity of such coherence peaks (relative to the autopeaks) with mixing time (T_m) may be due to the fact that they oscillate rapidly with T_m and/or generally exhibit different relaxation *vs* T_m.[58]

The receiver is based on the heterodyne principle, as noted above, and it detects quadrature signals in both CW and pulse modes. It has a bandwidth of 700 MHz.[13] The actual millimeter wave frequency is either referenced externally via a user-settable input or via a switch-selectable internal dielectric resonant oscillator (DRO). The external reference may be made frequency agile, and we are exploiting this feature as a means to perform pulsed ELDOR (PELDOR) experiments.[4,59] The bandwidth of the EIKA is sufficient (510 MHz) for these planned experiments.

Although, at present, complete spectral coverage is only available for motionally narrowed or highly ordered systems, useful pulse experiments may still be performed on systems with a spectral extent that is significantly greater than the available B_1. Possibilities for performing such experiments include field-swept electron spin-echo (FS-ESE) or other field-stepped spectroscopies.[53,60,61] The disadvantage of such experiments is that they sacrifice the so-called multiplex advantage (all signal channels excited simultaneously) as mentioned above. This is a particularly significant disadvantage for 2D-ELDOR experiments.[52,61] On the other hand, there may be situations in which partial excitation is sufficient to probe the interactions of interest.

For nitroxide spectra at or above 95 GHz, the **g**-tensor dominates spectral contributions over that from the hyperfine tensor. In the motional narrowing regime, the spectral extent is determined by the average hyperfine interaction and the average **g**-tensor, leading to a frequency-independent spectral extent of roughly ±1.5 mT (±15 G) and a frequency-dependent value of the central field. As one approaches the rigid limit for ESR frequencies higher than 95 GHz, the spectral extent increases approximately linearly with the ESR frequency. At 240 GHz, e.g. a rigid limit nitroxide spectrum has significant spectral weight

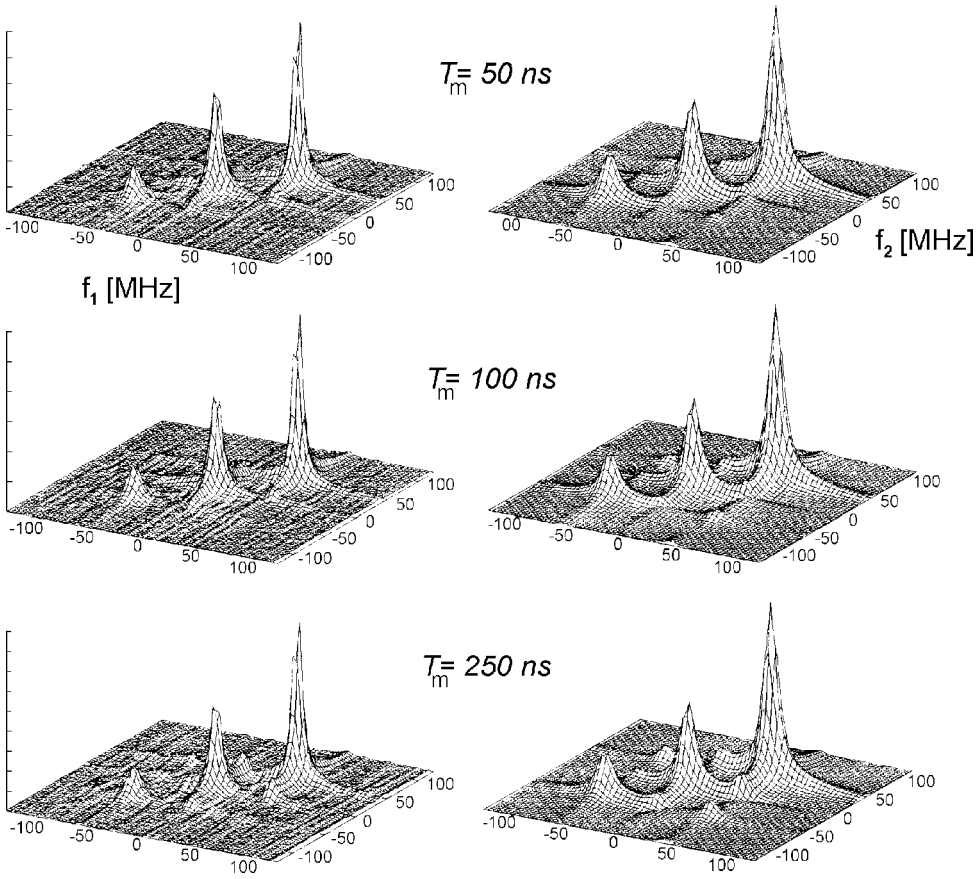

Figure 10. Experimental (left-hand side) and simulated (right-hand side) 2D-ELDOR-95 GHz S_{c-} spectra of 1 mM 4-acetamido-TEMPO solution in 90% water/10% glycerol at room temperature for various mixing times, T_m.[13]

Copyright © 2005 John Wiley & Sons, Ltd.

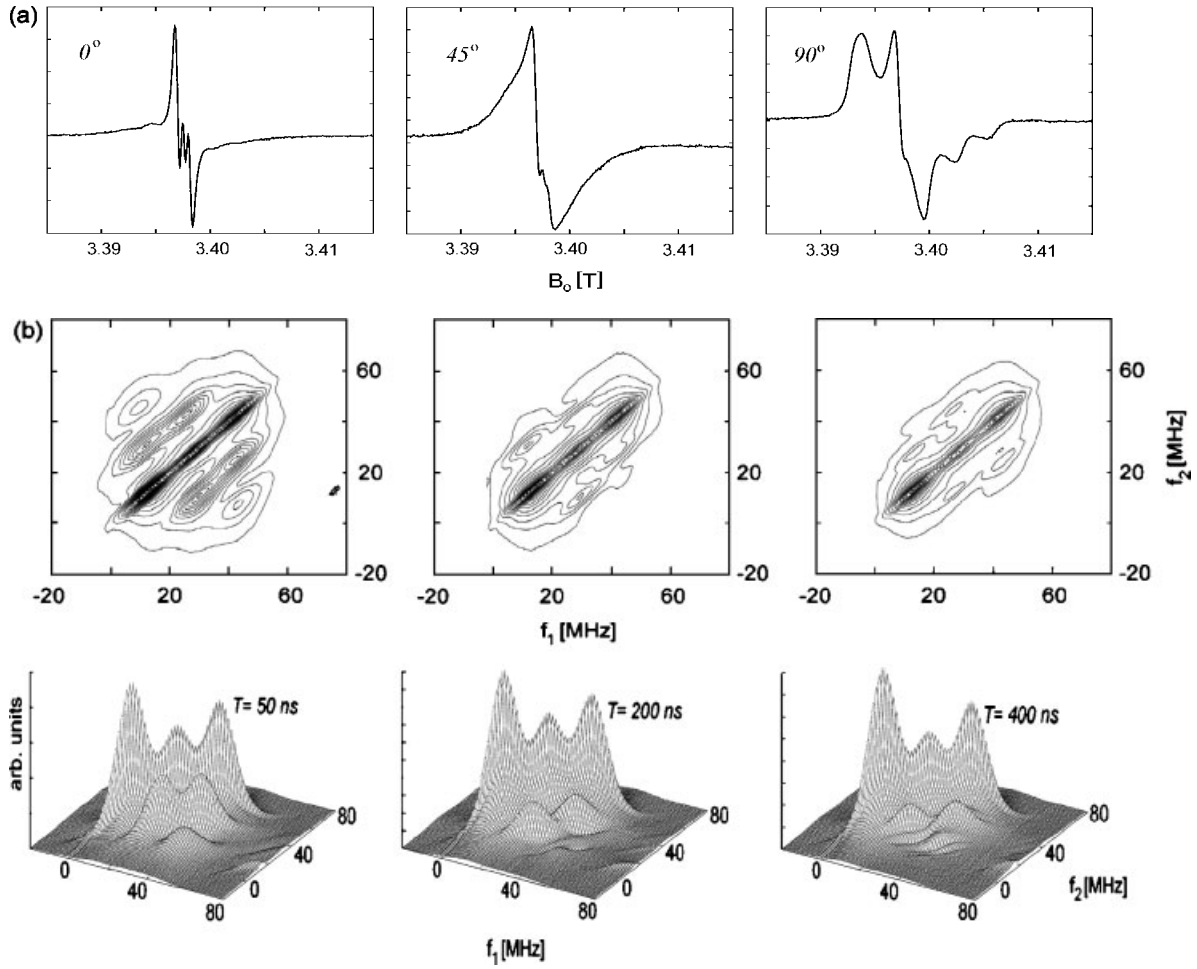

Figure 11. 2D-ELDOR at 95 GHz for cholestane (CSL) in oriented DPPC membranes at 17 °C. The CW spectra (a) are another demonstration of the microtome technique discussed in the text where samples were prepared with angles of $\psi = 0°$, 45° and 90° between the bilayer normal and the applied magnetic field. The 2D-ELDOR spectra (b) were taken for $\psi = 0°$ (director parallel to the applied magnetic field) at several mixing times. The upper plots in (b) are contours; the lower spectra are stack plots. Note that the lipid ordering, combined with the preferential alignment of the CSL magnetic *y*-axis to be (nearly) parallel to the director, constrains the spectral extent. In this case, the available B_1 is sufficient to excite the entire spectrum, since the spectral weight at the canonical *x*- and *z*-orientations are suppressed. Given that the available B_1 excites all of the relevant spin packets, the multiplex advantage obtains, and one observes true full-excitation 2D-ELDOR spectra. Note that the character of the off-diagonal peaks changes markedly as the mixing time increases.

over a range of ±19 mT (±190 G). Given that a 5 ns pulse corresponds to a B_1 of 1.7 mT (17 G), it would require a pulse of roughly 400 ps, corresponding to a B_1 of roughly 20 mT (200 G) to fully excite the entire spectrum.[60] We would also require an amplifier with larger instantaneous bandwidth to achieve such short pulses.

Nevertheless, we have found that even with a B_1 of 1.7 mT (17 Gauss) it is possible to obtain 2D-ELDOR spectra with reasonably good coverage at 95 GHz from nitroxide spin labels in the slow-tumbling regime, close to the rigid limit. The spectral bandwidth here is about ±175 MHz or ±6.2 mT (±62 G). We show spectra from spin-labeled gramicidin-A (GASl) in Fig. 12 that demonstrate this. Note that, owing to the finite available B_1 compared to the spectral extent, the coverage is nonuniform and decreases in the wings. The remarkable fact that such coverage is possible (for magnitude 2D spectra) has been discussed elsewhere[2,62] for 2D-FT-ESR at lower frequencies.

In Fig. 12, we show the 0° and 90° orientations of these aligned samples. The wide spectral extent compared to that of CSL in Fig. 11 is due to the fact that the GASl is less well aligned, although the significant differences in the spectra in Fig. 12 from the two orientations attests to the substantial ordering. What is most interesting is the fact that the spectral patterns change with mixing time. This is a clear indication that these 2D-ELDOR spectra show slow-motional effects, that is, the various dynamic spin packets,[20,54,60] relax at different rates, causing overall spectral changes as a function of the mixing time. These results are expected to provide insight into the detailed dynamics of gramicidin-A in the membrane.

SUMMARY

In this review, we have surveyed recent results from studies at high fields at ACERT, Cornell University. We

Copyright © 2005 John Wiley & Sons, Ltd.

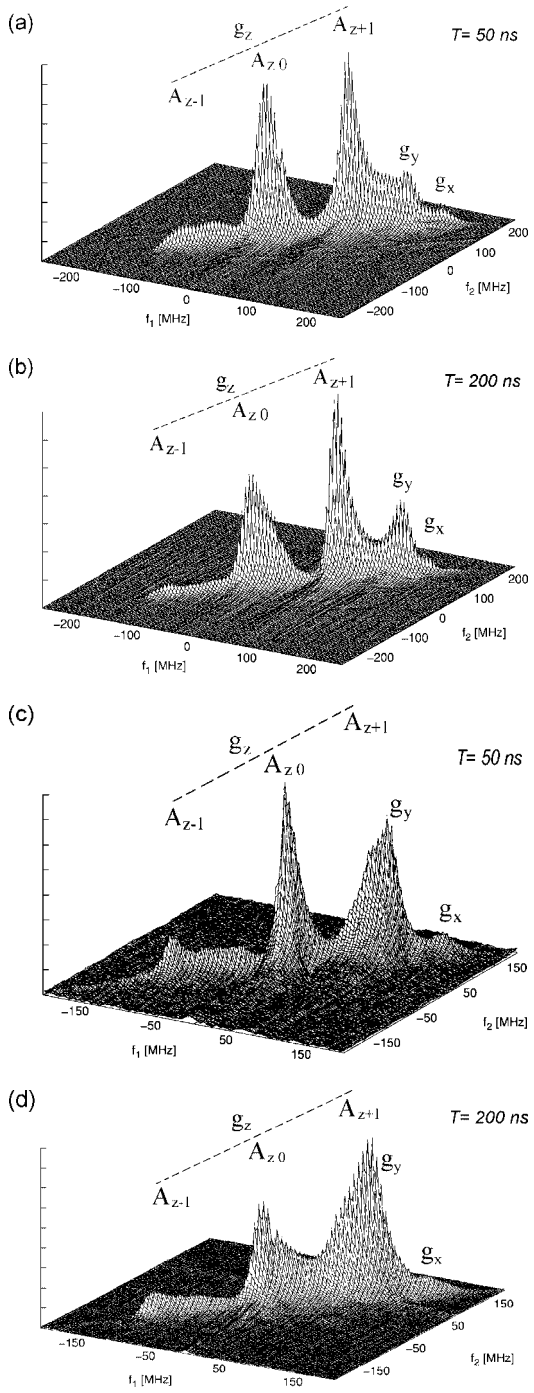

Figure 12. 2D-ELDOR spectra of gramicidin-A spin label (GASl) in aligned DPPC membranes at 7 °C: (a) and (b) have the director parallel to the applied field ($\psi = 0°$) with mixing times 50 and 200 ns, respectively; spectra in (c) and (d) have $\psi = 90°$ with the same mixing times, respectively. The spectral extent is approximately 350 MHz, corresponding to ±6 mT (±60 G). The B_1 in this case is about 1.7 mT (17 G). This yields imperfect coverage in the wings.

have also noted work at other high-field labs. Given the ever-growing range of significant scientific problems that high-field ESR is addressing, our approach here has been to focus on a few illustrative examples rather than strive for completeness. The collection of recently published review chapters edited by Grinberg and Berliner is a good place for further exploration of topics we have just touched on here.[63]

Acknowledgements

This work was supported by NIH/NCRR, NIH/NIBIB and NSF/Chemistry. We also acknowledge the use of the computational facilities of the Cornell University Theory Center during the preparation of this manuscript. We thank two anonymous reviewers whose comments and suggestions have helped us improve the paper.

REFERENCES

1. Budil DE, Earle KA, Lynch WB, Freed JH. Electron paramagnetic resonance at 1 millimeter wavelengths. In *Advanced EPR: Applications in Biology and Biochemistry*. Hoff AJ (ed.). Elsevier: Netherlands, 1989; chapt. 8.
2. Lebedev YaS. High–frequency continuous-wave electron spin resonance. In *Modern Pulsed and Continuous–Wave Electron Spin Resonance*, Kevan L, Bowman MK (eds). Wiley: New York, 1990; chapt. 8.
3. Earle KA, Budil DE, Freed JH. Millimeter wave electron spin resonance using quasioptical techniques. In *Advances in Magnetic and Optical Resonance*, vol. 19, Warren W (ed.). Academic: New York, 1996; 253.
4. Schweiger A, Jeschke G. *Principles of Pulse Electron Paramagnetic Resonance*, Clarendon Press: Oxford, 2001; chapt. 17.
5. Freed JH. The development of high-field/high-frequency ESR. In *Very High Frequency (VHF) ESR/EPR, Biological Magnetic Resonance*, vol. 22, Grinberg OYa, Berliner LJ (eds). Kluwer Academic/Plenum Publishers: New York, 2004; chapt. 2.
6. Fuchs MR, Prisner TF, Möbius. K. *Rev. Sci. Instrum.* 1999; **70**: 3681.
7. Hassan AK, Maniero AL, van Tol H, Saylor C, Brunel LC. *Appl. Magn. Reson.* 1999; **16**: 299.
8. Barra AL, Brunel LC, Robert JB. *Chem. Phys. Lett.* 1990; **165**: 107.
9. Virginia Diodes, Incorporation. http://www.virginiadiodes.com/ [last accessed June 2005].
10. CPI, Canada. http://www.cpii.com/cmp/index.asp [last accessed June 2005].
11. Thomas Keating Instruments and QMC Instruments. http://www.terahertz.co.uk/ [last accessed June 2005].
12. Bruker Biospin. http://www.bruker-biospin.com/brukerepr/index.html [last accessed June 2005].
13. Hofbauer W, Earle KA, Dunnam CR, Moscicki JK, Freed JH. *Rev. Sci. Instrum.* 2004; **75**: 1194.
14. Misra SK, Andronenko SI, Chand P, Earle KA, Paschenko SV, Freed JH. *J. Magn. Reson.* 2005; **174**: 265.
15. Smith GM, Lesurf JCG, Mitchell RH, Riedi PC. *Rev. Sci. Instrum.* 1998; **69**: 3924.
16. Blok H, Disselhorst JAJM, Orlinskii SB, Schmidt J. *J. Magn. Reson.* 2004; **166**: 92.
17. Columbus L, Hubbell W. *Trends Biochem. Sci.* 2002; **27**: 288.
18. Balog M, Kalai T, Jeko J, Berente Z, Steinhoff HJ, Engelhard M, Hideg K. *Tetrahedron Lett.* 2003; **44**: 9213.
19. Borbat PP, Costa-Filho AJ, Earle KA, Moscicki JK, Freed JH. *Science* 2001; **291**: 266.
20. Freed JH. *Annu. Rev. Phys. Chem.* 2000; **51**: 655.
21. Budil DE, Earle KA, Freed JH. *J. Phys. Chem.* 1993; **97**: 1294.
22. Fukui K, Ito T, Tada M, Aoyama M, Sato S, Onodera J, Ohya H. *J. Magn. Reson.* 2003; **163**: 174.
23. Hustedt EJ, Beth AH. *Biophys J.* 2004; **86**: 3940.
24. Liang ZC, Lou Y, Freed JH, Columbus L, Hubbell WL. *J. Phys. Chem. B* 2004; **108**: 17 649.
25. Liang ZC, Freed JH. *J. Phys. Chem. B* 1999; **103**: 6384.
26. Brune D, Kim S. *Proc. Natl. Acad. Sci. USA* 1993; **90**: 3835.
27. Barnes JP, Liang ZC, Mchaourab HS, Freed JH, Hubbell WL. *Biophys J.* 1999; **76**: 3298.
28. Polimeno A, Freed JH. *J. Phys. Chem.* 1995; **99**: 10 995.
29. Dzikovski BG, Borbat PP, Freed JH. *Biophys J.* 2004; **87**: 3504.

Copyright © 2005 John Wiley & Sons, Ltd.

30. Earle KA, Zeng R, Budil DE. *Appl. Magn. Reson.* 2001; **21**: 275.
31. Barnes JP, Freed JH. *Rev. Sci. Instrum.* 1997; **68**: 2838.
32. Barnes JP, Freed JH. *Rev. Sci. Instrum.* 1998; **69**: 3022.
33. Ge M, Budil DE, Freed JH. *Biophys J.* 1994; **67**: 2326.
34. Barnes JP, Freed JH. *Biophys J.* 1998; **75**: 2532.
35. Dzikovski BG, Earle KA, Pachtchenko S, Freed JH. Submitted to the *Journal of Magnetic Resonance*.
36. Earle KA, Smirnov AI. High field ESR: Applications to protein structure and dynamics In *Very High Frequency (VHF) ESR/EPR, Biological Magnetic Resonance, vol. 22*, OYa, Grinberg LJ, Berliner (eds). Kluwer Academic/Plenum Publishers: New York, 2004; chapt. 4.
37. Columbus L, Kalai T, Jeko J, Hideg K, Hubbell WL. *Biochemistry* 2001; **40**: 3828.
38. Goldsmith PF. *Quasioptical Systems: Gaussian Beam Quasioptical Propagation and Applications.* IEEE Press: Piscataway, NJ, 1998.
39. Hanson P, Martinez G, Millhauser G, Formaggio F, Crisma M, Toniolo C, Vita C. *J. Am. Chem. Soc.* 1996; **118**: 271.
40. Lesurf JCG ed. *Selected Papers on: Gaussian Beam Mode Optics for Millimeter-Wave and Terahertz Systems*. SPIE Press: Bellingham, 1993.
41. Earle KA, Tipikin DS, Freed JH. *Rev. Sci. Instrum.* 1996; **67**: 2502.
42. Teaney DT, Klein MP, Portis AM. *Rev. Sci. Instrum.* 1961; **32**: 721.
43. Bloch F, Hansen WW, Packard M. *Phys. Rev.* 1946; **70**: 474.
44. Budil DE, Earle KA. Sample resonators and quasioptical EPR In *Very High Frequency (VHF) ESR/EPR, Biological Magnetic Resonance, vol. 22*, Grinberg OYa, Berliner LJ (eds). Kluwer Academic/Plenum Publishers: New York, 2004; chapt. 11.
45. Earle KA, Freed JH. *Appl. Magn. Reson.* 1999; **16**: 247.
46. Prisner TF, Rohrer M, Möbius K. *Appl. Magn. Reson.* 1994; **7**: 167.
47. Hill S, Maccagnano S, Park K, Achey RM, North JM, Dalal NS. *Phys. Rev. B* 2002; **65**: 224 410.
48. Misra SK, Andronenko SI, Earle KA, Freed JH. *Appl. Magn. Reson.* 2001; **21**: 549.
49. Hofbauer W, Zouni A, Bittl R, Kern J, Orth P, Lendzian F, Fromme P, Witt HT, Lubitz W. *Proc. Natl Acad. Sci. USA* 2001; **98**: 6623.
50. Klette R, Törring JT, Plato M, Möbius K, Bonigk B, Lubitz W. *J. Phys. Chem.* 1993; **97**: 2015.
51. Borbat PP, Freed JH. *Chem. Phys. Lett.* 1999; **313**: 145.
52. Borbat PP, Crepeau RH, Freed JH. *J. Magn. Reson.* 1997; **127**: 155.
53. Schnegg A, Fuhs M, Rohrer M, Lubitz W, Prisner TF, Möbius. K. *J. Phys. Chem. B* 2002; **106**: 9454.
54. Freed JH. ESR and molecular dynamics In *Biomedical EPR, Part B: Methodology, Instrumentation and Dynamics, Biological Magnetic Resonance, vol. 24*, Eaton SS, Eaton GR, Berliner LJ, (eds). Kluwer Academic-Plenum Publications: New York, 2005; 239; chapt. 9.
55. Schneider DJ, Freed JH. Calculating slow-motional magnetic resonance spectra: A user's guide. In *Biological Magnetic Resonance*, vol. 8, Berliner L, Reuben J (eds). Plenum Press: New York, 1989; 1.
56. ELVA-1 Millimeter Wave Division. http://www.elva-1.com [last accessed June 2005].
57. Chandler C. *J. Appl. Phys.* 1949; **20**: 1188.
58. Lee S, Patyal BR, Freed JH. *J. Chem. Phys.* 1993; **98**: 3665.
59. Milov AD, Salikhov KM, Shirov MD. *Sov. Phys. Solid State* 1981; **24**: 565.
60. Millhauser GL, Freed JH. *J. Chem. Phys.* 1984; **81**: 37.
61. Gorcester J, Millhauser GL, Freed JH. Two dimensional ESR. In *Modern Pulsed and Continuous-Wave Electron Spin Resonance*, Kevan L, Bowman MK (eds). Wiley: New York, 1990; chap. 3.
62. Hornak JP, Freed JH. *J. Magn. Reson.* 1986; **67**: 501.
63. Grinberg OYa, Berliner LJ (eds). Very High Frequency (VHF) ESR/EPR *Biological Magnetic Resonance*, vol. 22, Kluwer Academic/Plenum Publishers: New York, 2004.

Copyright © 2005 John Wiley & Sons, Ltd.